Virtual multi-antenna array for estimating the direction of a transmitter: system, bounds and experimental results

François Quitin, Philippe De Doncker, François Horlin and Wee Peng Tay

***Abstract*—A method is proposed to estimate the direction of a radio-frequency (RF) transmitter with a mobile, single-antenna receiver. By considering the received signal at several points along its trajectory, the receiver implicitly creates a virtual multi-antenna array, which can be used to estimate the direction of the transmitter. Virtual arrays differ from conventional multi-antenna arrays in two ways: 1) the position and orientation of each antenna in the virtual array depends on the movement of the receiver and is not known *a priori*; and 2) the local oscillator (LO) frequency offset between transmitter and receiver adds a phase offset to the signal received by each antenna of the virtual array, which must be estimated and compensated. The first problem is solved by using an inertial measurement unit (IMU), which can provide the relative position of the receiver for short time durations. The second problem is solved by estimating the LO frequency offset jointly with the direction of the transmitter by extending the MUSIC algorithm for multi-dimensional estimation. We investigate the Cramér-Rao lower bound (CRLB) of the proposed estimator, which provides some insights in the design of our system. We implement our system on a software-defined radio testbed, and present some measurement result obtained in a controlled environment.**

***Index Terms*—Virtual antenna array, Direction of Arrival, RF localization**

I. Introduction

Localization of radio frequency (RF) transmitters is a crucial component of modern wireless networks, with applications in commercial and military fields, such as vehicular wireless networks, 5G cellular network, autonomous robotics and navigation systems [1]. This is especially important when Global Navigation Satellite System (GNSS) is not available, such as in dense urban environments, tunnels or indoors. One method for determining the location of the RF transmitter is by estimating it's bearing with respect to multiple access points. Multi-antenna arrays have proven to be an efficient method for estimating the Direction-of-Arrival (DoA) of a RF transmitter. The main drawback of multi-antenna arrays is the high cost and large form factors associated with such arrays, making them unsuitable for portable consumer electronics. In this paper we investigate the feasibility of DoA estimation of a RF transmitter with a *mobile, single-antenna* receiver. By considering successive received packets at different points along the receiver trajectory, we implicitly recreate a *virtual* antenna array which can be used to estimate the DoA of the RF transmitter, as shown in Figure 1. These periodic received packets could be the Primary Synchronization Signal (PSS) sent by the base station in LTE, or the frames transmitted by a roadside unit in a 802.11p vehicular scenario. The difficulty of such a method is twofold: 1) the cumulative phase due to local oscillator (LO) frequency offset needs to be removed for DoA estimation to become feasible; and 2) the relative positions of the receiver needs to be estimated with high accuracy (a fraction of a wavelength) to know the location of the "virtual" antenna elements. The significance of our work lies in the feasibility of our DoA estimation method with cheap, off-the-shelf hardware, which is already readily available in modern smartphones. Our work has the potential to revolutionize DoA estimation (and thus localization) of portable consumer electronics.

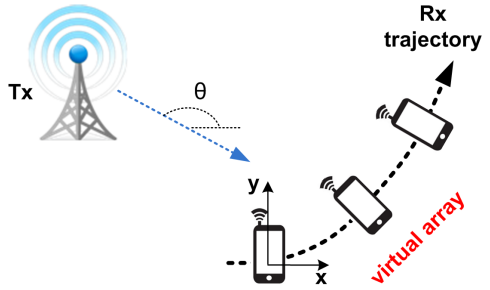

Fig. 1. Virtual DoA estimation concept.

Contributions: The contributions of this paper can be summarized as follows.

- We propose a system to estimate the direction of a RF transmitter using a *mobile, single-antenna* receiver. The system proposes practical, realistic solutions to account for hardware limitations;
- we deduce the Cramér-Rao lower bound (CRLB) of the proposed estimator. It is shown that at high SNRs, the CRLB of our system approaches the CRLB of a conventional multi-antenna array;
- the proposed system is implemented on an proof-of-concept experimental testbed, and results in a controlled

F. Quitin, P. De Doncker and F. Horlin are with the Brussels School of Engineering, Universté libre de Bruxelles (ULB), Belgium ({fquitin, pdedonck, fhorlin}@ulb.ac.be). W.P. Tay is with the School of Electrical and Electronic Engineering, Nanyang Technological University (NTU), Singapore (wptay@ntu.edu.sg)

environment show that the system behaves according to the theoretical predictions.

Compared to our previous conference paper [2], we propose a new estimator to evaluate the LO frequency offset and DoA jointly, further building on our previous work The new estimator is an extension of the MUSIC algorithm for multi-dimensional estimation. It is more accurate and does not suffer from the disadvantages of nonlinear optimization methods. Additionally, we also calculate the CRLB of the proposed estimator.

Related work: DoA estimation with multi-antenna array has led to several DoA estimation techniques, such as beamforming [3], [4], [5], Multiple Signal Classification (MUSIC) [6], [7], [8], [9], [10], Estimation of Signal Parameters via Rotational Invariance Techniques (ESPRIT) [11], [12], [13], or unitary ESPRIT [14]. These different techniques offer different trade-offs in complexity, accuracy and resolution [15], [16]. Note that DoA can also be used in combination with other metrics to achieve accurate localization [17]. Another class of DoA estimation methods are maximum likelihood (and Bayesian methods for tracking), where different mulitpath components of wireless channels are estimated [18],[19] and tracked [20],[21].

Multi-antenna arrays, however, suffer from multiple disadvantages. One main disadvantage is the large form factor that is required: antennas need to be separated by typically half a wavelength [22], which results in physically large systems unsuitable for portable consumer electronics. Another disadvantage is the requirement to calibrate the antenna array, which can be a difficult and cumbersome process [23]. A final disadvantage is the cost associated to having multiple RF and/or baseband chains for each antenna, significantly increasing the overall cost of the DoA estimation system.

One method for DoA estimation with single-antenna systems was proposed in [24], [25], which uses a rotating directional antenna. The DoA is then determined as the direction from which the received signal strength is maximized. The drawback of such system is the need for a directional antenna, which usually comes with large form factor, and the need to rotate the antenna, which requires a servo motor or a dedicated movement.

Another closely related technology is bistatic synthetic aperture radar (SAR), where a (static) receiver uses the signal transmitted by a satellite (and reflected by the environment) to reconstruct a radar image of the illuminated environment [26], [27], [28]. The direct signal between the satellite and the receiver is used to calibrate for the LO frequency offset, and can be separated from the environment-reflections by using high bandwidth and high-gain directional antennas. The use of *virtual* multi-antenna arrays has been widely adopted in wireless channel sounding for some time [29], [30], [31], [32], and is usually performed by 1) synchronizing the transmitter and receiver through RF cables and 2) using precise mechanical devices to move the transmit and/or receive antenna to the required positions in the virtual array.

More flexible virtual multi-antenna arrays have also been considered for DoA estimation and positioning in [33], [34], [35][36]. These works focus on estimating the DoA of multipath components with virtual arrays, and in [37] the CRLB of the DoA estimated with a virtual array is computed. While the use of inertial measurement units to determine the relative position of the receiver is similar to our work, these papers suppose very low values for the LO frequency offset (values around 0.1 Hz). The experimental results are achieved by using a high-end channel sounder, where both transmitter and receiver are equipped with rubidium local oscillators so that any LO frequency offset is negligible [38], [35][36]. By contrast, the virtual array DoA estimation method presented in this paper aims at being feasible with cheap, off-the-shelf hardware, which typically has significant LO frequency offset between the transmitter and the receiver. Moreover, the work in [35] uses particle filters to perform long-term tracking of the different states to observe (i.e. the DoA of the different transmitters or multipath components). Such filters typically take some time to converge (around ten seconds in [35]), and are sensitive to successions of poor estimates (e.g. if the transmitter is hidden by an obstacle). In this work, we describe a method that uses a limited observation of the signal to estimate the DoA, that is only conditioned on a short observation (i.e. a few seconds) of the radio signal.

II. DoA estimation system

A. Virtual antenna array

DoA algorithms rely on interferometry, i.e. analyzing the phase differences between the multiple antenna elements of the receiver. Therefore, our system model will include non-idealities that affect the phase of the different "virtual" antennas in our system. The non-idealities that affect the phase of a received signal are the transmitter and receiver front-end phase offset, as well as the frequency offset between transmitter and receiver, both of which will be detailed below. We assume that the receiver is operated in it's linear regime, to avoid any non-linear phase distortions. We ignore the effect of LO phase noise [39], as it's influence on the proposed estimator is negligible.

We consider a transmitter sending an RF signal in the form of digital data packets. The preamble of the packets is known by both the transmitter and the receiver, and is determined by the communication standard (e.g. the primary synchronization sequence in 3G systems or the short/long preamble in 802.11 systems)[1]. The packets sent by the transmitter may or may not be periodic. The receiver correlates its received baseband samples with the known preamble in order to determine the boundaries of the received packets.

Let us denote $s[m]$ the baseband representation of the transmitted packet header (for $m = 1, ..., M$) and $r[n, m]$ the m-th baseband sample of the n-th received packet, which can be represented as:

$$r[n,m] = h[n,m] * s[m] \cdot e^{j(\varphi_0 + 2\pi f_0 (t_n + mT_s))} + w[n,m] \quad (1)$$

where $h[n, m]$ is the wireless channel impulse response, φ_0 is the phase of the initial received packet (which contains

[1]Note that the proposed system would also work for narrowband signals.

the phase offset and accumulated frequency offset at time t_0 between the transmitter and the receiver front-ends), f_0 is the frequency offset between the transmitter and the receiver due to LO frequency offset, t_n is the time elapsed between the initial packet and the n-th packet, T_s is the receiver sample time, and $w[n,m]$ is an independent and identically distributed (i.i.d.) Gaussian noise with distribution $w[n,m] \sim \mathcal{CN}(0,\sigma_n^2)$. Note that (1) implicitly assumes that the frequency offset f_0 does not change over time, which is approximately true for short periods of time: a few seconds for a temperature-controlled crystal oscillator (TCXO), a few tens of seconds for an oven-controlled crystal oscillator (OCXO). If the transmitter up-conversion chain and the receiver down-conversion chain (both analog and digital) are not turned off between the considered packets (which is the case for modern transceivers), the term φ_0 will remain constant between multiple received packets.

We focus on narrowband, line-of-sight channel, therefore $h[n,m]$ is defined as

$$h[n,m] = \alpha e^{j\vec{\beta}\cdot\vec{r}[n]} \tag{2}$$

where α is the amplitude of the channel, $\vec{\beta}$ is the wave vector and $\vec{r}[n]$ are the receiver coordinates when receiving the n-th packet with respect to (w.r.t.) the receiver coordinates when receiving the initial packet.

Without loss of generality, we consider two-dimensional arrays (in the x-y plane), and propagation in the horizontal plane, ignoring elevation. We can then make the following simplification:

$$\vec{\beta}\cdot\vec{r}[n] = \frac{2\pi}{\lambda}\left(x[n]\cos(\theta) + y[n]\sin(\theta)\right) \tag{3}$$

where θ is the azimuth-of-arrival of the transmitter, λ is the wavelength at the carrier frequency, and $x[n], y[n]$ are the $x-$ and $y-$coordinates of the receiver when receiving the n-th packet (the origin of the coordinate system are the coordinates of the receiver when receiving the initial packet). Combining (1), (2) and (3), we have

$$\begin{aligned} r[n,m] = \alpha \cdot s[m] \\ \cdot e^{j\left(\varphi_0 + 2\pi f_0(t_n + mT_s) + \frac{2\pi}{\lambda}(x[n]\cos(\theta) + y[n]\sin(\theta))\right)} \\ + w[n,m]\,. \end{aligned} \tag{4}$$

Our goal is to leverage on DoA estimation techniques that are readily available for conventional multi-antenna arrays. The main difference between (4) and the signal at each antenna in a conventional multi-antenna system is the term $2\pi f_0 t_n$. Additionally, the position of the receiver $(x[n], y[n])$ at each packet receive time depends on the movement of the receiver, unlike a conventional multi-antenna receiver where the positions of the antennas in the array are fixed. Two main tasks thus need to be performed to leverage on conventional multi-antenna array processing results:

1) The position of the receiver at each period $x[n], y[n]$ needs to be estimated, with an accuracy of a fraction of a wavelength.
2) The frequency offset f_0 needs to be estimated and compensated for in the received signal.

The DoA can then be estimated using traditional multi-antenna array processing techniques, such as MUSIC [6], ESPRIT [11] or unitary ESPRIT [14].

B. Receiver position estimation

The first difficulty of virtual arrays lies in estimating the relative position of the receiver along its trajectory. Besides the relative position (which requires an accuracy of a fraction of a wavelength), the orientation of the receiver also needs to be estimated to account for non-isotropic antenna radiation patterns. This rules out conventional GNSS systems, which do not meet the required accuracy and do not provide orientation information.

Note that the movement range (and hence duration) should be quite limited, as to stay in the wide-sense stationary uncorrelated scattering (WSSUS) assumptions required for multi-antenna array processing. Because of this short movement constraint, it is sufficient to use a 3-dimensional (3D) inertial measurement unit (IMU) to estimate the relative movement of the receiver. A 3D IMU contains 3D accelerometers and 3D gyroscopes, which can be used to obtain the relative position and orientation of the receiver through dead-reckoning integration methods (as shown in Figure 2). Note that using IMU processing requires to know the initial orientation of the receiver, as well as the initial speed of the receiver. In this work, we assume that these are available through continuous tracking from an initial stand-still position [40]. The origins of the coordinate system is considered to be the initial position, as only the relative position is required. The conventional methods for integrating IMU data is through an extended Kalman filter (EKF) or Unscented Kalman filter (UKF), which provides a 3D navigation solution [40].

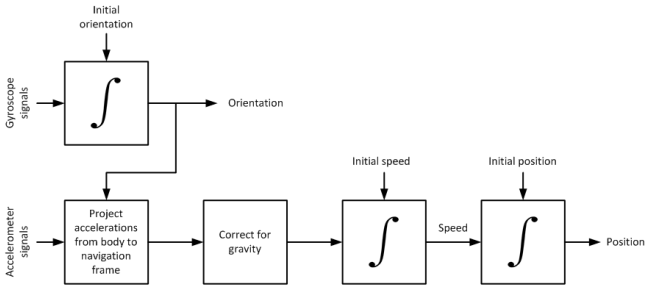

Fig. 2. Steps of IMU dead-reckoning processing process.

Due to the integration of biases in the IMU processing, the navigation solution obtained from IMU measurements will drift from the real trajectory and the error of the navigation solution will increase over time. However, for the WSSUS assumption to hold, the time over which the receiver forms the virtual array should be short, so that the navigation error incurred by the IMU is usually small. For pedestrian or vehicular speed, the movement duration is typically limited to a few seconds.

C. LO frequency offset compensation

The second challenge of virtual antenna arrays is to estimate and compensate the LO frequency offset in (4). In [2], we

proposed a Stop-and-Start (SaS) approach, where the receiver first stands still before starting to move. During standstill, only the LO frequency offset causes the phase to change in (4), and can easily be estimated. This estimated value is then used during the movement of the receiver to compensate the LO frequency offset. This method suffers from two disadvantages. The most obvious disadvantage is that the SaS approach restricts the movement of the receiver, as the receiver first needs to stand still before moving. The second disadvantage is that the LO frequency offset should not change too much between the moment the receiver stands still and the moment the receiver starts moving, which might not always be verified in practice (especially for low-quality LOs). A method was proposed in [2] to jointly estimate the LO frequency offset and the DoA, but this relied on black-box optimization with little convergence guarantees and poor accuracy.

In this paper, we extend the MUSIC algorithm to the joint estimation of LO frequency offset and DoA. Note that while we use the MUSIC algorithm in this paper, the signal model below could be applied to any type of DoA estimation algorithm, such as beamforming, ESPRIT, unitary ESPRIT, etc. Also note that subspace based methods such as MUSIC or ESPRIT are not statistically efficient [41], [42], and that ML based method should provide better performances. We apply the MUSIC algorithm with an adapted signal model, that takes into account the LO frequency offset. Let us rewrite (4) by stacking the N received packets in a column vector:

$$\mathbf{y}[m] = \mathbf{a}(f_0, \theta)x[m] + \mathbf{w}[m] \tag{5}$$

with $\mathbf{a}(f_0, \theta)$ the steering vector (containing the LO frequency offset) defined as

$$\mathbf{a}(f_0, \theta) = \begin{bmatrix} e^{j\left(2\pi f_0 t_1 + \frac{2\pi}{\lambda}(x[1]\cos(\theta)+y[1]\sin(\theta))\right)} \\ e^{j\left(2\pi f_0 t_2 + \frac{2\pi}{\lambda}(x[2]\cos(\theta)+y[2]\sin(\theta))\right)} \\ \vdots \\ e^{j\left(2\pi f_0 t_N + \frac{2\pi}{\lambda}(x[N]\cos(\theta)+y[N]\sin(\theta))\right)} \end{bmatrix} \tag{6}$$

and $x[m]$ constant for all virtual antennas, defined as

$$x[m] = \alpha \cdot s[m] \cdot e^{j(\varphi_0 + 2\pi f_0 m T_s)} \tag{7}$$

and $\mathbf{w}[m] = [w[1,m], w[2,m], \dots w[N,m]]^T$ the $N \times 1$ white Gaussian noise vector, with covariance matrix $\mathbf{R_n} = \sigma_n^2 \mathbf{I}_N$

Conventional DoA estimation algorithms, such as beamforming or MUSIC, can be used with the signal model (5). Let us define $\mathbf{S} = \mathbb{E}\{\mathbf{y}\mathbf{y}^*\}$ the $N \times N$ covariance matrix, where $\mathbb{E}\{\cdot\}$ and $(\cdot)^*$ are the expectation and the Hermitian operator, respectively. In the case of the MUSIC algorithm, we search for the K components orthogonal to the noise subspace [6] (if there is only one signal source, $K = 1$). Let $\mathbf{E_w}$ be the $N \times (N-K)$ matrix of eigenvectors corresponding to the $(N-K)$ smallest eigenvalues of $\mathbf{S}$. The MUSIC spectrum is defined as

$$P_{\text{MU}}(f_0, \theta) = \frac{1}{\mathbf{a}^*(f_0, \theta)\mathbf{E_w}\mathbf{E_w}^*\mathbf{a}(f_0, \theta)} \tag{8}$$

Similarly to the beamforming case, f_0 and θ can be estimated with a two-dimensional search:

$$\left(\hat{f_0}, \hat{\theta}\right) = \arg\max_{(f_0,\theta)} \left\{P_{\text{MU}}(f_0, \theta)\right\} \tag{9}$$

Note that in the case of multiple signals (e.g. in the case of multipath components), the MUSIC algorithm offers a much better resolution than simple beamforming [6].

D. Receiver movement constraints

Conventional multi-antenna systems need to satisfy the spatial Nyquist criterion, i.e. the distance between antenna elements must be smaller than $\lambda/2$ where λ is the wavelength at the carrier frequency [22]. In a virtual multi-antenna system, the distance traveled by the receiver between two successive packets must be smaller than $\lambda/2$. This translates to the constraint $v_r\,(t_n - t_{n-1}) < \lambda/2$, where v_r is the speed of the receiver. In the following, we will consider transmitters that send periodic packets, such that $t_n = nT_0$, where T_0 is the transmit period. In that case, the constraint becomes

$$v_r < \frac{\lambda}{2T_0} \tag{10}$$

As an illustration, let us consider the case of a 3G signal. A 3G base station sends a primary synchronization sequence every 0.667 ms, and has a carrier frequency of 2.1 GHz. This would lead to a maximum receiver speed of 107 m/s (or 385 km/h), showing that the virtual DoA estimation method is applicable when the receiver is mounted on a typical ground vehicle. Note that while this is true for all conventional RF frequencies, this might no longer be true for millimeter-wave systems. At 60 GHz, the wavelength is reduced to 5 mm. Using equation (10) with a 0.667 ms packet period, we can see that the maximum speed is reduced to 13.5 km/h. This means that the proposed system would be unsuitable for mobile millimeter-wave systems. Another constraint of our system is that (similarly to conventional multi-antenna arrays), a linear trajectory results in an DoA ambiguity: the real DoA will be θ or $\pi - \theta$. Finally note that non-stationary channels will cause distortion of the multipath components, which cannot be recovered with a virtual array. However, as long as the transmitter remains static during the receiver movement, and only the transmitter's direction is estimated, this should not cause any problem for the proposed system.

III. Bounds of virtual array DoA estimation

We evaluate the CRLB for a virtual antenna array, when the position of the virtual antennas are estimated through IMU processing. We start by deriving the CRLB in section III-A, and in section III-B we analyze the virtual antenna position error resulting from IMU dead-reckoning processing. The aim of deriving the CRLB is to provide a tool to be able to quickly compare different configurations of system parameters and/or receiver trajectories.

A. Derivation of the CRLB

Let us simplify the received signal (5) by considering $s[m] = 1$ and $\varphi_0 = 0$, and the LO frequency offset within a single packet is compensated (using the packet header) such that $2\pi f_0 m T_s$ disappears from the phase term. Moreover, we assume the transmitter sends a periodic signal, such that $t_n = nT_0$, where T_0 is the transmit period. While signal periodicity is not a requirement for our virtual DoA estimation method, it simplifies the derivation of the CRLB presented in this section. Therefore, the CRLB derivation presented below is only valid for periodic signals. With the previous assumptions, the simplified received signal is given by

$$\mathbf{y} = \mathbf{a}(f_0, \theta)x + \mathbf{w} \tag{11}$$

with $x = \alpha$ and

$$\mathbf{a}(f_0,\theta) = \begin{bmatrix} e^{j\left(2\pi f_0 T_0 + \frac{2\pi}{\lambda}(x[1]\cos(\theta)+y[1]\sin(\theta))\right)} \\ e^{j\left(2\pi f_0 2T_0 + \frac{2\pi}{\lambda}(x[2]\cos(\theta)+y[2]\sin(\theta))\right)} \\ \vdots \\ e^{j\left(2\pi f_0 NT_0 + \frac{2\pi}{\lambda}(x[N]\cos(\theta)+y[N]\sin(\theta))\right)} \end{bmatrix} \tag{12}$$

and $\mathbf{w}$ the $N \times 1$ i.i.d. white Gaussian noise vector, with covariance matrix $\mathbf{R_n} = \sigma_n^2 \mathbf{I}_N$. The coordinates $[x[1], x[2], ..., x[N]]^T$ and $[y[1], y[2], ..., y[N]]^T$ are the *true* position of the virtual antennas

The *estimated* antenna position (after IMU dead-reckoning processing) are given by $(x[n] + \delta x_n, y[n] + \delta y_n)$, where δx_n and δy_n are i.i.d. zero-mean white Gaussian noise processes with variances $\sigma^2_{x_n}$ and $\sigma^2_{y_n}$, respectively. The unknown parameters of our system are the frequency offset f_0, the DoA θ, and the antenna position errors δx_n and δy_n (for $n = 1, ..., N$). There are thus $2 + 2N$ unknown parameters, which can be stacked in a vector $\mathbf{\Theta}$:

$$\mathbf{\Theta} = [f_0, \theta, \delta x_1, \delta y_1, \delta x_2, \delta y_2, ..., \delta x_N, \delta y_N] \tag{13}$$

The probability density function of the received signal can be expressed as

$$p(\mathbf{y}; \mathbf{\Theta}) = \frac{1}{\pi^N \det(\mathbf{R_n})} e^{-(\mathbf{y}-\mathbf{a}(f_0,\theta)x)^* \mathbf{R_n}^{-1} (\mathbf{y}-\mathbf{a}(f_0,\theta)x)} \tag{14}$$

Note that $\mathbf{\Theta}$ is composed of two deterministic unknown parameters and $2N$ random unknown parameters. In this case, the Fisher information matrix can be defined as [43], [37]

$$\mathbf{I}(\mathbf{\Theta})_{ij} = \mathbf{I}_1(\mathbf{\Theta})_{ij} + \mathbf{I}_2(\mathbf{\Theta})_{ij} \tag{15}$$

with $1 \leq i, j \leq 2 + 2N$, and the two elements of the Fisher information matrix defined as

$$\mathbf{I}_1(\mathbf{\Theta})_{ij} = -\mathbb{E}_{\mathbf{y_s},\mathbf{\Theta}} \left[\frac{\partial^2 \ln p(\mathbf{y}; \mathbf{\Theta})}{\partial \mathbf{\Theta}_i \partial \mathbf{\Theta}_j} \right] \tag{16}$$

$$\mathbf{I}_2(\mathbf{\Theta})_{ij} = -\mathbb{E}_{\mathbf{\Theta}} \left[\frac{\partial^2 \ln p(\mathbf{\Theta})}{\partial \mathbf{\Theta}_i \partial \mathbf{\Theta}_j} \right] \tag{17}$$

The different terms of matrix $\mathbf{I}_1(\mathbf{\Theta})$ can be determined, and are derived in Appendix A. They depend on several system parameters (e.g. T_0, σ_n^2, λ), the DoA θ and the receiver trajectory (e.g. $x[n]$ and $y[n]$). The second part of the Fisher information matrix $\mathbf{I}_2(\mathbf{\Theta})$ has a simpler structure, and only depends on the position variances [43]:

$$\mathbf{I}_2(\mathbf{\Theta}) = \begin{bmatrix} \mathbf{0}_{2\times 2} & \mathbf{0}_{2\times 2N} \\ \mathbf{0}_{2N\times 2} & \mathbf{\Sigma}^{-1}_{2N\times 2N} \end{bmatrix} \tag{18}$$

where $\mathbf{\Sigma}$ is a diagonal matrix containing the variances of the positioning errors on its diagonal, defined as

$$\mathbf{\Sigma} = \text{diag}\left(\sigma^2_{x_1}, \sigma^2_{y_1}, \sigma^2_{x_2}, \sigma^2_{y_2}, ..., \sigma^2_{x_N}, \sigma^2_{y_N}\right) \tag{19}$$

The next section focuses on determining those positioning error variances, based on the most important IMU errors. Note that this derivation of the CRLB assumes uncorrelated errors in the estimation of the receiver trajectory. IMU integration produces correlated errors, which causes the CRLB to be too optimistic. However, the relative comparison of different receiver trajectories and/or system parameters remains applicable. Also note that the CRLB remains valid for other types of receiver trajectory estimation methods (e.g. high-accuracy differential GNSS systems), requiring only to update the elements of $\mathbf{I}_2$ in (18).

B. IMU integration position error

The navigation solution provided by combining and processing IMU signals (such as illustrated in Section II-B) is plagued by several errors. The variance of these errors need to be evaluated to fill the elements of $\mathbf{\Sigma}$ in (19). Given the short integration times considered in this paper (typically a few seconds), we only consider the following noise sources:

- white Gaussian noise on the accelerometers and gyroscopes;
- biases on the accelerometers and gyroscopes;
- errors in the estimation of the initial orientation.

While biases are present in any IMU (regardless of the IMU quality), these can be measured quite accurately and compensated for in the measured signals [44]. Estimating the initial orientation of the IMU lies outside the scope of this paper, but in practice, using the Earth's gravitational field at standstill can provide a good estimate of the orientation of the receiver [45] (tracking filters can then be used to keep the updated orientation of the receiver; as the gyroscope signals are integrated only once, the orientation of the receiver stays accurate for reasonably long periods).

The Gaussian noise errors in the accelerometers and gyroscopes result in two types of errors. Errors in the accelerometer signals are double-integrated in the IMU dead-reckoning process (as shown in Figure 2). The double-integration of a white Gaussian noise results in a second-order random walk process [46]. The error in the navigation solution then has a variance given by

$$\sigma^2_{\text{acc},n} = \sigma_a^2 T_i \frac{(nT_0)^3}{3} \tag{20}$$

where σ_a^2 is the accelerometer noise variance and T_i is the IMU (and thus accelerometer) sampling time.

Errors in the gyroscope signals are singly-integrated in the IMU dead-reckoning process and cause a misorientation ϵ_n, whose variance is given by

$$\sigma^2_{\epsilon_n} = \sigma^2_g T_i(nT_0) \tag{21}$$

where σ^2_g is the gyroscope noise variance. An orientation error of ϵ_n results in a component of the gravitation vector g to be projected onto the horizontal axes when compensating for g (see Figure 2). The component of g projected onto the horizontal axes yields a bias error equal to $g\sin(\epsilon_n)$, which for small ϵ_n is approximately equal to $g \cdot \epsilon_n$. The double-integration of an acceleration bias results in an error in the horizontal plane equal to

$$\epsilon_{xy,n} = \epsilon_n \cdot g \cdot \frac{(nT_0)}{2} \tag{22}$$

The variance of $\epsilon_{xy,n}$ is then given by

$$\sigma^2_{\text{orien},n} = \sigma^2_g T_i(nT_0)\left[g\frac{(nT_0)}{2}\right]^2 \tag{23}$$

Finally, the total positioning error of the IMU processing due to accelerometer and gyroscope noises then has a total variance of

$$\sigma^2_{x_n} = \sigma^2_{y_n} = \sigma^2_{\text{acc},n} + \frac{1}{2}\sigma^2_{\text{orien},n} \tag{24}$$

where the error due to projection of the gravitation vector on the horizontal plane is split equally between the x- and y-axes. These values can be used to fill the elements of $\mathbf{\Sigma}$ in (19) to compute our system's CRLB.

TABLE I
SYSTEM PARAMETERS

Parameter	Value
Movement	Semi-circle, $R = \{30, 40, 50\}$ cm
Movement duration	5 s
Center frequency	1 GHz
T_0	100 ms
Accelerometer noise density	80 $\mu g/\sqrt{\text{Hz}}$
Accelerometer bandwidth	375 Hz
Gyroscope noise density	0.03 $^\circ/s/\sqrt{\text{Hz}}$
Gyroscope bandwidth	415 Hz
IMU sample rate	200 Hz

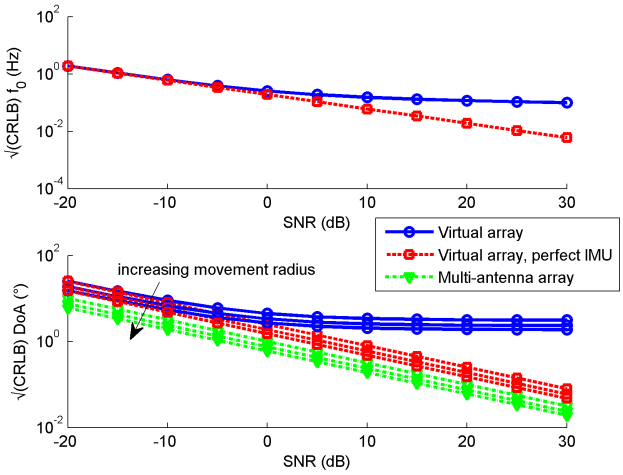

Fig. 3. CRLB of the proposed system.

C. CRLB results

The CRLB of our system ("Virtual array") is evaluated and compared to two situations: one where LO frequency offset is still present, but the positions of the virtual antennas are known exactly ("Virtual array, perfect IMU"); and one where there is no LO frequency offset and the positions of the virtual antennas are known exactly, corresponding to the situation of an ideal multi-antenna array ("Multi-antenna array"). The parameters of our system are described in Table I. The generated movements and system parameters are set to match our experimental setup presented in Section IV. The receiver first accelerates, then decelerates, along a semi-circle. The distance between virtual antennas varies between a few millimeters to at most 8 cm (depending on the phase of acceleration or deceleration). The IMU parameters correspond to the XSens-MTI 10 IMU, which will be used in our experiments, and can be found in the IMU's datasheet.

Figure 3 shows the CRLB of f_0 and θ, and compares it to the case with perfect IMU and of an ideal multi-antenna array, for different movement sizes. Since the ideal multi-antenna array does not have frequency offset between its antenna elements, only the CRLB of θ is provided. It can be seen that, for moderate to high SNR levels, the CRLB of our estimator is only marginally higher than that of an ideal multi-antenna array. Note that in the generated scenario, there are 40 "virtual" antennas. The equivalent multi-antenna array would require 40 antenna elements, which would be prohibitive in realistic scenarios. Additionally, it can be observed that larger movements yield lower CRLBs, which is consistent with conventional multi-antenna array theory, where physically larger array offer better resolution and improved DoA estimation performance. Compared to a conventional multi-antenna array, a virtual multi-antenna array (with perfect IMU) has a systematic performance offset. This is due to the fact that the frequency offset estimation contains some error, which also decreases with increasing SNR. The CRLB of a virtual antenna arrays with a realistic IMU, however, reaches a performance floor at high SNRs. This is due to limited IMU performances: if the position of the virtual antennas contains some error, higher SNR levels will not help improve estimation performances. This shows that limited IMU performances is a main limiting factor of virtual multi-antenna arrays.

D. Multipath channels: simulation results

In this section, we evaluate the effect of multipath components on our virtual multi-antenna array DoA estimation through simulations. Similarly to Section III-C, the system parameters (see Table I) and receiver movements are set to match the experiments in Section IV. The line-of-sight (LoS) component to the transmitter has a unit amplitude, and a random DoA between 60° and 120°. An additional N_{MPC} multipath components are added to the LoS, in which case (2)

becomes

$$h[n,m] = e^{j\vec{\beta}\cdot\vec{r}[n]} + \sum_{k=1}^{N_{MPC}} \alpha_k e^{j(\varphi_k + \vec{\beta_k}\cdot\vec{r}[n])} \quad (25)$$

where φ_k is a random phase term distributed uniformly over $[0, 2\pi[$, β_k is the wave vector of the k-th multipath component (corresponding to a DoA that is distributed uniformly over $[0, 2\pi[$), and α_k is the amplitude of the k-th multipath component. The amplitude of each multipath component is distributed uniformly over $[0, \alpha_{\max}]$. The number of multipath components N_{MPC} was set to ten in our simulations. This corresponds to a worst-case scenario, where the multipath component's DoAs are distributed evenly over all angles.

Monte-Carlo simulations are performed to determine the effect of different levels of multipath power, i.e. by varying $\alpha_{\max}$. The processing methods that are used to integrate the IMU signals are described in Sections II-B and IV-B. We compare the SaS approach and the joint estimator proposed in Section II-C. Figure 4 shows the result of the simulation. As can be expected, for low multipath powers the performances of the system are very good (and close to the CLRB). When the multipath power reaches within 10 dB of the LoS power, the performances start to degrade, for both the SaS approach and the joint estimator.

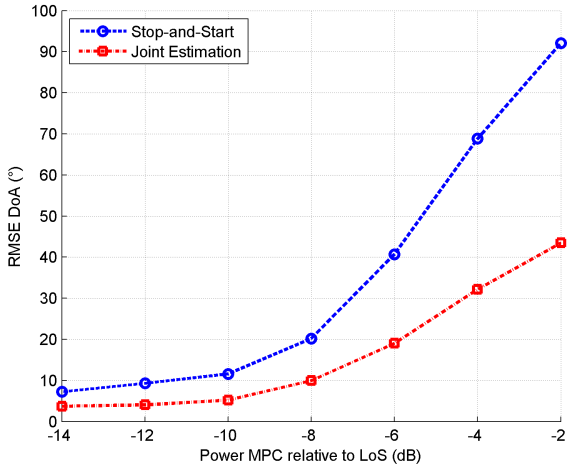

Fig. 4. DoA RMSE versus multipath component power.

IV. Experimental setup and results

A. Experimental setup

The proposed system was tested on a hardware platform in an anechoic chamber. Both the transmitter and receiver were composed of USRP-N210 software-defined radios, equipped with a WBX 50-2200 MHz daughterboard and a GPSDO module. The GPSDO module is equipped with a high-accuracy oven-controlled crystal oscillator (OCXO) that can bypass the USRPs internal temperature-controlled crystal oscillator (TCXO), increasing the LO accuracy from a few ppm (parts-per-million) to 20 ppb (parts-per-billion). The transmitter sends a periodic 3G primary synchronization sequence every 0.667 ms. The carrier frequency is set to 1 GHz. The receiver performs correlation between the transmitted sequence and its received baseband signal in real-time (in the USRP FPGA, as this operation cannot be performed in real-time in software), and accumulates the correlated signals over 3 packets to increase the SNR of the correlated signal, yielding an SNR of 15 to 20 dB. Finally, a peak detector function in the host processor detects the peaks in the correlation function, thereby finding the boundaries of the received packet, which is recorded to a data file. The IMU used in this experiment is an XSens-MTi 10, automotive-grade IMU. It contains 3D-acellerometers, 3D-gyroscopes and 3D-magnetometers (the latter are not used in this work). The data from the IMU is recorded in the same data file as the received packets by a separate thread. The receiver antenna and the IMU are

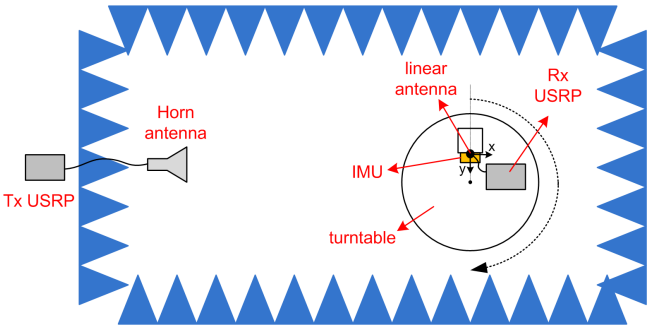

Fig. 5. Top view of the experimental setup in the anaechoic chamber.

attached to the turntable of the anechoic chamber as shown in Figure 5. The IMU is placed with the z-axis parallel to the vertical axis, although slight misorientation (typically a few degrees) cannot be avoided in practice. During each experiment run, the receiver is first standing still for 30 s. After the standstill phase, the turntable (and thus the receiver and IMU) is rotated by $180°$, which takes about 5 s. The receiver and IMU have been placed at a radius of approximately 30, 40 and 50 cm of the turntable center. For each radius, the experiment was repeated 10 times. Attaching the receiver to the anechoic chamber turntable allows to know exactly which movement was generated (the turntable has a precision that is below $0.5°$). This allows us to evaluate the performance of the IMU processing algorithms, described in the next section. The anechoic chamber turntable did not allow us to modify the rotation speed or the type of movement (e.g. translation) of the receiver.

B. IMU processing

The IMU measurements are converted to a relative position by using the Unscented Kalman Filter (UKF) proposed in [40]. The UKF implements the steps shown in Figure 2, and requires the initial pitch and roll of the receiver (the original yaw is supposed to be at 0, and the DoA will be given w.r.t. the original yaw)[2]. In our experiments, the initial pitch and roll

[2]in navigation literature, yaw represents the orientation around the z-axis, pitch is the orientation around the x-axis and roll is the orientation around the y-axis

of the IMU are estimated using the technique proposed in [45], which uses the observation that during standstill only the gravitation vector is measured by the accelerometers. The static biases of the accelerometers were estimated prior to the experiment, while the biases of the gyroscopes are estimated during the standstill phase. In all of the experimental results, it is observed that towards the end of the movement, the navigation solution drifts off from the ground truth. This is mostly due to small errors in estimating the initial pitch/roll, or due to small errors in the accelerometer bias calibration. Figure 6 shows the IMU processing for one realization of the experiment. The first two subfigures show the values measured by the accelerometers and gyroscopes, respectively. It can be seen that the accelerometer readings are dominated by the gravitation vector ($g = 9.78$ m/s^2 along the vertical axis), but a slight acceleration and deceleration along the $x-$axis are observed. The gyroscope clearly shows a rotation around the $z-$axis. The third and fourth subfigures show the orientation

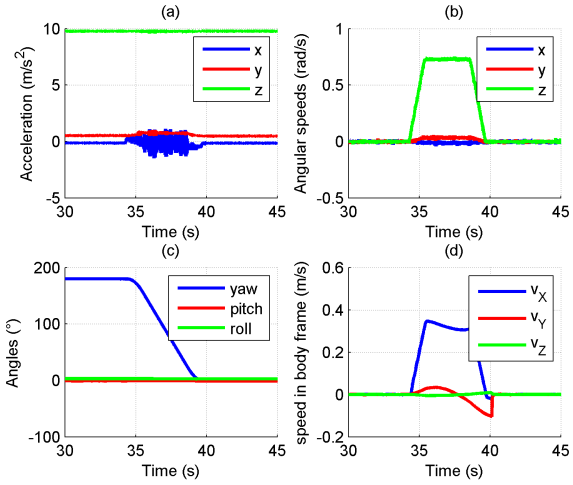

Fig. 6. IMU processing: (a) accelerometer measurements, (b) gyroscope measurements, (c) UKF solution for the IMU orientation and (d) UKF solution for the IMU speeds (in the body frame)

and speeds (in the body frame) of the IMU after running the UKF. It can be seen that the IMU's yaw changes from $180°$ to $0°$, which matches the movement that was generated with the turntable. The speeds are mainly along the $x-$axis of the IMU, which again is consistent with the movement generated by the turntable. The slight speeds along the IMU $y-$axis are due to the initial misorientation of the IMU and the integration errors of the UKF. The position error of the navigation solution provided by the IMU UKF (at the end of the movement) has been measured, and is given in Table II. Note that this is the error *at the end of the movement*, i.e. the error is usually close to zero for the first few seconds of movement, and then increases fast during the later instants of the movement.

C. Results and analysis

Two techniques are investigated for DoA estimation. The first one is the SaS approach from [2], where the receiver is first at standstill before moving. The received packets are used to estimate the frequency offset f_0 during standstill, and the received packets during movement are then compensated for f_0. The second technique is the joint estimation algorithm presented in Section II-C, where the MUSIC algorithm is applied using the adapted signal model.

TABLE II
IMU UKF POSITION ERROR AT THE END OF THE MOVEMENT OVER 10 EXPERIMENT RUNS.

Movement Radius	Mean error	std. error
30 cm	25 cm	16 cm
40 cm	15 cm	8 cm
50 cm	14 cm	7 cm

Figure 7 shows the results of the SaS approach for one realization of the experiment. Fig. 7(a) shows the phase of the received packets before frequency offset compensation. Due to the frequency offset, the phase shift due to the movement of the receiver cannot be observed. However, after compensating for the frequency offset, the phase shift due to the movement can clearly be observed, as shown in Fig. 7(b). The phase variations before the movement (0∼30 s) are mostly due to the local oscillator drift between the transmitter and the receiver. Fig. 7(c) shows the IMU-estimated navigation solution. It can be seen that the navigation solution is not a perfect half-circle, but drifts off towards the end of the movement, for the reasons mentioned above. Finally, Fig. 7(d) shows the MUSIC spectrum which is used to estimate the DoA. A clear peak is observed at $94°$, which is close to the true DoA of $90°$.

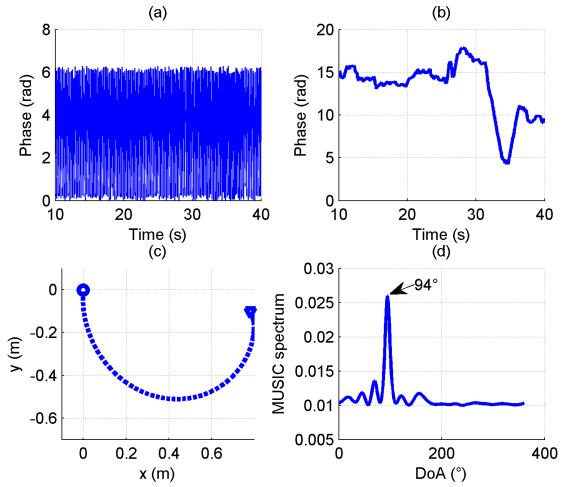

Fig. 7. Experimental results of the SaS approach: (a) phase measurements before frequency offset compensation, (b) phase measurements after frequency offset compensation, (c) UKF solution for the IMU trajectory and (d) MUSIC spectrum with an estimated DoA of $94°$

Figure 8 shows the results of the joint estimation approach for one realization of the experiment. In this experiment, only the received packets during receiver movement were used for processing. Subfigure (a) shows the two-dimensional MUSIC spectrum (versus f_0 and θ). The peak of the spectrum indicates the estimated values for f_0 and θ. Subfigure (b) shows a horizontal cut of the MUSIC spectrum at the value of f_0

TABLE III
DOA RMSE OVER 10 EXPERIMENT RUNS.

Movement Radius	Stop-and-Start	Joint estimation
30 cm	13.70°	28.22°
40 cm	8.08°	16.55°
50 cm	6.19°	6.18°

corresponding to the peak. A clear peak (similar to the MUSIC spectrum of the SaS approach) can be identified at 96°, close to the true DoA of 90°. Finally, subfigure (c) shows the estimated IMU trajectory. The circles indicate the location of the "virtual" antennas.

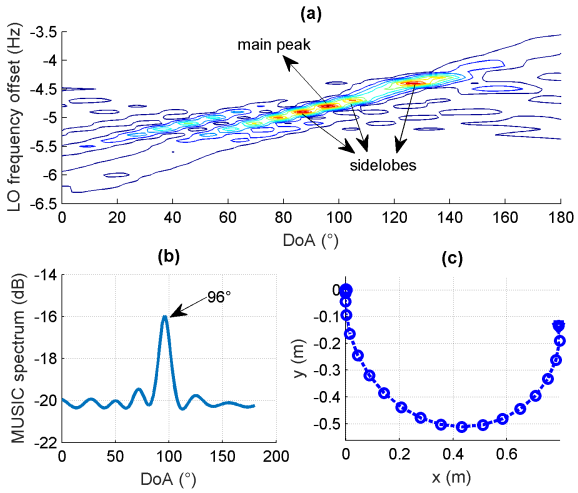

Fig. 8. Experimental results of the joint estimation approach: (a) 2D-MUSIC spectrum, (b) MUSIC spectrum at the LO frequency corresponding to the peak, and (c) UKF solution for the IMU trajectory.

For both the SaS approach and the joint estimation approach, the mean of the DoA estimation over all measurement runs is zero. The root mean square error (RMSE) for different movement radiuses are shown in Table III. It can be seen that better results are obtained for larger radiuses. This is consistent with conventional multi-antenna array theory, where a better resolution is obtained for physically larger arrays. Measurements where the IMU UKF has a large positioning error tend to have large DoA estimation error, but for measurements with a positioning error smaller than 30 cm (at the end of the movement) no strong correlation appears between the UKF positioning error and the DoA error. The results of the joint estimation are worse than those in the SaS case, especially for small movement radiuses. This can be attributed to the fact that the joint estimation uses less samples (it only uses the samples from when the receiver is actually moving), but also due to the lesser performance of the joint estimator. The advantage is that there is no need to stop the receiver before the movement. Such an usage flexibility comes at the cost of a decreased estimation accuracy. Note that the joint estimator also requires more computation power to perform the two-dimensional search over f_0 and θ. The estimation performance of the LO frequency offset cannot be evaluated, as the real LO frequency offset between transmitter and receiver is unknown. The SaS approach estimates the LO frequency offset at standstill, which is very reliable, but the true LO frequency offset might drift between the standstill and the movement phase. However, the difference in the estimated LO frequency offset between the SaS and joint estimation approach can be evaluated. Both methods provide LO frequency offsets that are very close, in the order of $5 \sim 10$ Hz for our experiments, consistent with the OCXO specifications, with a mean difference of 0.04 Hz (and a standard deviation of the difference of 0.15 Hz).

While this error can be considered high with respect to conventional multi-antenna arrays, it needs to be reminded that this is a fundamental shift from conventional multi-antenna DoA estimation theory. We are trying to estimate DoA with a single-antenna receiver, which requires to also estimate and compensate LO frequency offset. In that respect, it can be expected that performances would decrease. We believe that further optimization of the LO offset/DoA estimation methods is possible, and that better processing of the IMU data can be performed to improve DoA estimation performances, but this is beyond the scope of this paper.

Finally, it can be observed that the measurement error is higher than the CRLB. The measurements were performed at SNRs of 15 to 20 dB. The CRLB at these SNRs is 2° for a movement radius of 50 cm, 2.5° for a movement radius of 40 cm, and 3° for a movement radius of 30 cm, all of which are significantly lower than the measured RMSE (6°, 16° and 28° respectively). This is mainly due because the CRLB assumes uncorrelated errors, while errors in our case are correlated over time. However, the relative comparison of different receiver trajectories and/or system parameters remains applicable.

V. CONCLUSION

A promising method was proposed to estimate the DoA of a RF transmitter with a mobile, single-antenna receiver. By considering several packets along its trajectory, the receiver creates a virtual multi-antenna array that can use conventional DoA estimation algorithms. The relative position of the receiver is estimated through IMU dead-reckoning, while the phase rotation due to LO offset between transmitter and receivers is estimated jointly with the DoA by adapting the signal model. The CRLB of our virtual multi-antenna system was evaluated, and shown to match closely to conventional multi-antenna DoA systems. Experimental results in an anechoic chamber show the feasibility of the proposed method. Our future work will focus on evaluating and improving the robustness of the proposed method, in order to account for low-grade IMUs, low-quality LOs and multipath environments.

APPENDIX A
DERIVATION OF THE ELEMENTS OF MATRIX $\mathbf{I}_1(\boldsymbol{\Theta})$

Deriving (16) using (14) provides the following result:

$$\mathbf{I}_1(\boldsymbol{\Theta})_{ij} = -\mathbb{E}_{\mathbf{y},\boldsymbol{\Theta}}\left[\frac{\partial^2 \ln p(\mathbf{y};\boldsymbol{\Theta})}{\partial\boldsymbol{\Theta}_i \partial\boldsymbol{\Theta}_j}\right] \tag{26}$$

$$= \frac{\partial \mathbf{a}^H}{\partial\boldsymbol{\Theta}_i}\mathbf{R_n}^{-1}\frac{\partial \mathbf{a}}{\partial\boldsymbol{\Theta}_j} + \frac{\partial \mathbf{a}^H}{\partial\boldsymbol{\Theta}_j}\mathbf{R_n}^{-1}\frac{\partial \mathbf{a}}{\partial\boldsymbol{\Theta}_i} \tag{27}$$

where $\mathbf{\Theta}_i, \mathbf{\Theta}_j$ are the elements of $\mathbf{\Theta}$, $\mathbf{a}$ is the signal model in (12), and $\mathbf{R_n}$ is the covariance matrix of the noise term in (11).

Deriving for the different individual terms of $\mathbf{I}_1(\mathbf{\Theta})$, we obtain the following.

$$-\mathbb{E}_{\mathbf{y},\mathbf{\Theta}}\left[\frac{\partial^2 \ln p(\mathbf{y};\mathbf{\Theta})}{\partial f_0^2}\right] = \frac{2}{\sigma_n^2}(2\pi T_0)^2 \sum_{k=1}^{N} k^2 \tag{28}$$

$$-\mathbb{E}_{\mathbf{y},\mathbf{\Theta}}\left[\frac{\partial^2 \ln p(\mathbf{y};\mathbf{\Theta})}{\partial \theta^2}\right] = \frac{2}{\sigma_n^2}\left(\frac{2\pi}{\lambda}\right)^2 \sum_{k=1}^{N} \left(x[k]\sin(\theta) - y[k]\cos(\theta)\right)^2 \tag{29}$$

$$-\mathbb{E}_{\mathbf{y},\mathbf{\Theta}}\left[\frac{\partial^2 \ln p(\mathbf{y};\mathbf{\Theta})}{\partial f_0 \partial \theta}\right] = \frac{2}{\sigma_n^2}(2\pi T_0)\left(\frac{2\pi}{\lambda}\right) \sum_{k=1}^{N} k\left(-x[k]\sin(\theta) + y[k]\cos(\theta)\right) \tag{30}$$

$$-\mathbb{E}_{\mathbf{y},\mathbf{\Theta}}\left[\frac{\partial^2 \ln p(\mathbf{y};\mathbf{\Theta})}{\partial \delta x_n \partial \delta x_m}\right] = \begin{cases} \frac{2}{\sigma_n^2}\left(\frac{2\pi}{\lambda}\right)^2 \cos^2(\theta) & \text{if } n = m \\ 0 & \text{if } n \neq m \end{cases} \tag{31}$$

$$-\mathbb{E}_{\mathbf{y},\mathbf{\Theta}}\left[\frac{\partial^2 \ln p(\mathbf{y};\mathbf{\Theta})}{\partial \delta y_n \partial \delta y_m}\right] = \begin{cases} \frac{2}{\sigma_n^2}\left(\frac{2\pi}{\lambda}\right)^2 \sin^2(\theta) & \text{if } n = m \\ 0 & \text{if } n \neq m \end{cases} \tag{32}$$

$$-\mathbb{E}_{\mathbf{y},\mathbf{\Theta}}\left[\frac{\partial^2 \ln p(\mathbf{y};\mathbf{\Theta})}{\partial \delta x_n \partial \delta y_m}\right] = \begin{cases} \frac{2}{\sigma_n^2}\left(\frac{2\pi}{\lambda}\right)^2 \sin(\theta)\cos(\theta) & \text{if } n = m \\ 0 & \text{if } n \neq m \end{cases} \tag{33}$$

$$-\mathbb{E}_{\mathbf{y},\mathbf{\Theta}}\left[\frac{\partial^2 \ln p(\mathbf{y};\mathbf{\Theta})}{\partial f_0 \partial \delta x_n}\right] = \frac{2}{\sigma_n^2}(2\pi T_0)\left(\frac{2\pi}{\lambda}\right) n\cos(\theta) \tag{34}$$

$$-\mathbb{E}_{\mathbf{y},\mathbf{\Theta}}\left[\frac{\partial^2 \ln p(\mathbf{y};\mathbf{\Theta})}{\partial f_0 \partial \delta y_n}\right] = \frac{2}{\sigma_n^2}(2\pi T_0)\left(\frac{2\pi}{\lambda}\right) n\sin(\theta) \tag{35}$$

$$-\mathbb{E}_{\mathbf{y},\mathbf{\Theta}}\left[\frac{\partial^2 \ln p(\mathbf{y};\mathbf{\Theta})}{\partial \theta \partial \delta x_n}\right] = \frac{2}{\sigma_n^2}\left(\frac{2\pi}{\lambda}\right)^2 \left(-x[n]\sin(\theta) + y[n]\cos(\theta)\right)\cos(\theta) \tag{36}$$

$$-\mathbb{E}_{\mathbf{y},\mathbf{\Theta}}\left[\frac{\partial^2 \ln p(\mathbf{y};\mathbf{\Theta})}{\partial \theta \partial \delta y_n}\right] = \frac{2}{\sigma_n^2}\left(\frac{2\pi}{\lambda}\right)^2 \left(-x[n]\sin(\theta) + y[n]\cos(\theta)\right)\sin(\theta) \tag{37}$$

The other elements can be obtained by noting that $\mathbf{I}_1(\mathbf{\Theta})$ is a symmetric matrix.

ACKNOWLEDGMENTS

The authors would like to acknowledge the financial support of the David and Alice Van Buuren fund.

REFERENCES

[1] N. Patwari, J. N. Ash, S. Kyperountas, A. O. Hero, R. L. Moses, and N. S. Correal, "Locating the nodes: cooperative localization in wireless sensor networks," *IEEE Signal Processing Magazine*, vol. 22, no. 4, 2005.

[2] Francois Quitin, Vivek Govindaraj, Xionghu Zhong, and Wee Peng Tay, "Virtual multi-antenna array for estimating the angle-of-arrival of a RF transmitter," in *Proc. 2016 IEEE 84th Vehicular Technology Conference (VTC2016-Fall)*, September 2016.

[3] Darren B. Ward, Zhi Ding, and R.A. Kennedy, "Broadband DOA estimation using frequency invariant beamforming," *Signal Processing, IEEE Transactions on*, vol. 46, no. 5, pp. 1463–1469, May 1998.

[4] M. Wax and Y. Anu, "A least squares approach to blind beamforming," *Signal Processing, IEEE Transactions on*, vol. 47, no. 1, pp. 231–234, Jan 1999.

[5] C.J. Lam and A.C. Singer, "Bayesian Beamforming for DOA Uncertainty: Theory and Implementation," *Signal Processing, IEEE Transactions on*, vol. 54, no. 11, pp. 4435–4445, Nov 2006.

[6] R. Schmidt, "Multiple emitter location and signal parameter estimation," *IEEE Transactions on Antennas and Propagation*, vol. 34, no. 3, pp. 276–280, Mar 1986.

[7] Mostafa Kaveh and A. Barabell, "The statistical performance of the MUSIC and the minimum-norm algorithms in resolving plane waves in noise," *Acoustics, Speech and Signal Processing, IEEE Transactions on*, vol. 34, no. 2, pp. 331–341, Apr 1986.

[8] B. Porat and Benjamin Friedlander, "Analysis of the asymptotic relative efficiency of the MUSIC algorithm," *Acoustics, Speech and Signal Processing, IEEE Transactions on*, vol. 36, no. 4, pp. 532–544, Apr 1988.

[9] G.M. Kautz and M.D. Zoltowski, "Performance analysis of MUSIC employing conjugate symmetric beamformers," *Signal Processing, IEEE Transactions on*, vol. 43, no. 3, pp. 737–748, Mar 1995.

[10] F.G. Yan, M. Jin, and X. Qiao, "Low-Complexity DOA Estimation Based on Compressed MUSIC and Its Performance Analysis," *Signal Processing, IEEE Transactions on*, vol. 61, no. 8, pp. 1915–1930, April 2013.

[11] A. Paulraj, R. Roy, and T. Kailath, "A subspace rotation approach to signal parameter estimation," *Proceedings of the IEEE*, vol. 74, no. 7, pp. 1044–1046, July 1986.

[12] B. Ottersten and T. Kailath, "Direction-of-arrival estimation for wide-band signals using the ESPRIT algorithm," *Acoustics, Speech and Signal Processing, IEEE Transactions on*, vol. 38, no. 2, pp. 317–327, Feb 1990.

[13] F. Gao and A.B. Gershman, "A generalized ESPRIT approach to direction-of-arrival estimation," *Signal Processing Letters, IEEE*, vol. 12, no. 3, pp. 254–257, March 2005.

[14] M. Haardt and J. A. Nossek, "Unitary esprit: how to obtain increased estimation accuracy with a reduced computational burden," *IEEE Transactions on Signal Processing*, vol. 43, no. 5, pp. 1232–1242, May 1995.

[15] Petre Stoica and Arye Nehorai, "Performance comparison of subspace rotation and MUSIC methods for direction estimation," *Signal Processing, IEEE Transactions on*, vol. 39, no. 2, pp. 446–453, Feb 1991.

[16] Jeong-Geun Hong, Chan-Sik Park, and Bo-Seok Seo, "Comparison of MUSIC and ESPRIT for direction of arrival estimation of jamming signal," in *Instrumentation and Measurement Technology Conference (I2MTC), 2012 IEEE International*, May 2012, pp. 1741–1744.

[17] Wenji Xu, Francois Quitin, Mei Leng, Wee Peng Tay, and Sirajudeen G. Razul., "Distributed localization of a RF target in NLOS environments," *IEEE J. Sel. Areas Commun.*, vol. 33, no. 7, pp. 1–14, 2015.

[18] B. H. Fleury, M. Tschudin, R. Heddergott, D. Dahlhaus, and K. Ingeman Pedersen, "Channel parameter estimation in mobile radio environments using the sage algorithm," *IEEE Journal on Selected Areas in Communications*, vol. 17, no. 3, pp. 434–450, Mar 1999.

[19] J. Salmi, A. Richter, and V. Koivunen, "Detection and tracking of MIMO propagation path parameters using state-space approach," *IEEE Trans. Signal Process.*, vol. 57, no. 4, 2009.

[20] T. Jost, W. Wang, U.-C. Fiebig, and F. Perez-Fontan, "Detection and Tracking of Mobile Propagation Channel Paths," *IEEE Trans. Ant. and Prop.* , vol. 60, no. 10, 2012.

[21] G. E. Kirkelund, G. Steinbock, X. Yin, and B. Fleury, "Tracking of the temporal behaviour of path components in the radio channel - a comparison between methods," in *2008 Annual IEEE Student Paper Conference*, Feb 2008, pp. 1–5.

[22] Bruno Clerckx and Claude Oestges, *MIMO Wireless Networks: Channels, Techniques and Standards for Multi-Antenna, Multi-User and Multi-Cell Systems*, Academic Press: Oxford, UK, 2013.

[23] Srikanth Pagadarai, Travis Collins, and Alexander Wyglinski, "Direction Finding with the USRP X-Series and TwinRX," Tech. Rep., Ettus Research, Application Note AN-244, 2016.

[24] J. Graefenstein, A. Albert, P. Biber, and A. Schilling, "Wireless node localization based on RSSI using a rotating antenna on a mobile robot," in *Positioning, Navigation and Communication, 2009. WPNC 2009. 6th Workshop on*, March 2009, pp. 253–259.

[25] J.T. Isaacs, F. Quitin, L.R. Garcia Carrillo, U. Madhow, and J.P. Hespanha, "Quadrotor control for RF source localization and tracking," in *Int. Conf. on Unmanned Aircraft Syst. (ICUAS)*, May 2014, pp. 244–252.

[26] F. Comblet, A. Khenchaf, A. Baussard, and F. Pellen, "Bistatic synthetic aperture radar imaging: Theory, simulations, and validations," *IEEE Transactions on Antennas and Propagation*, vol. 54, no. 11, pp. 3529–3540, Nov 2006.

[27] A. Moreira, P. Prats-Iraola, M. Younis, G. Krieger, I. Hajnsek, and K. P. Papathanassiou, "A tutorial on synthetic aperture radar," *IEEE Geoscience and Remote Sensing Magazine*, vol. 1, no. 1, pp. 6–43, March 2013.

[28] R. Wang, Y. Deng, Z. Zhang, Y. Shao, J. Hou, G. Liu, and X. Wu, "Double-channel bistatic sar system with spaceborne illuminator for 2-d and 3-d sar remote sensing," *IEEE Transactions on Geoscience and Remote Sensing*, vol. 51, no. 8, pp. 4496–4507, Aug 2013.

[29] S. Ranvier, M. Kyro, K. Haneda, T. Mustonen, C. Icheln, and P. Vainikainen, "VNA-based wideband 60 GHz MIMO channel sounder with 3-D arrays," in *Radio and Wireless Symposium, 2009. RWS '09. IEEE*, Jan 2009, pp. 308–311.

[30] F. Quitin, C. Oestges, F. Horlin, and P. De Doncker, "Polarization measurements and modeling in indoor NLOS environments," *Wireless Communications, IEEE Transactions on*, vol. 9, no. 1, pp. 21–25, January 2010.

[31] F. Quitin, C. Oestges, F. Bellens, S. van Roy, F. Horlin, and P. De Doncker, "Model parametrization and validation for specular-diffuse clustered channel models," *Antennas and Propagation, IEEE Transactions on*, vol. 60, no. 8, pp. 4019–4022, Aug 2012.

[32] Y. Miao, K. Haneda, M. Kim, and J. Takada, "Antenna de-embedding of radio propagation channel with truncated modes in the spherical vector wave domain," *Antennas and Propagation, IEEE Transactions on*, vol. 63, no. 9, pp. 4100–4110, Sept 2015.

[33] M. A. Yaqoob, F. Tufvesson, A. Mannesson, and B. Bernhardsson, "Direction of arrival estimation with arbitrary virtual antenna arrays using low cost inertial measurement units," in *2013 IEEE International Conference on Communications Workshops (ICC)*, June 2013, pp. 79–83.

[34] M. A. Yaqoob, A. Mannesson, N. R. Butt, and F. Tufvesson, "Source localization using virtual antenna arrays," in *2015 International Conference on Location and GNSS (ICL-GNSS)*, June 2015, pp. 1–6.

[35] A. Mannesson, M. A. Yaqoob, B. Bernhardsson, and F. Tufvesson, "Tightly coupled positioning and multipath radio channel tracking," *IEEE Transactions on Aerospace and Electronic Systems*, vol. 52, no. 4, pp. 1522–1535, August 2016.

[36] C. Gentner, R. Poehlmann, M. Ulmschneider, T. Jost, and S. Zhang, "Positioning using terrestrial multipath signals and inertial sensors," *Mobile Information Systems*, 2017.

[37] M. A. Yaqoob, A. Mannesson, B. Bernhardsson, N. R. Butt, and F. Tufvesson, "On the performance of random antenna arrays for direction of arrival estimation," in *2014 IEEE International Conference on Communications Workshops (ICC)*, June 2014, pp. 193–199.

[38] A. Mannesson, M. A. Yaqoob, F. Tufvesson, and B. Bernhardsson, "Radio and imu based indoor positioning and tracking," in *2012 19th International Conference on Systems, Signals and Image Processing (IWSSIP)*, April 2012, pp. 32–35.

[39] C. Zucca and P. Tavella, "The clock model and its relationship with the allan and related variances," *IEEE Transactions on Ultrasonics, Ferroelectrics, and Frequency Control*, vol. 52, no. 2, pp. 289–296, Feb 2005.

[40] Rudolph van der Merwe, Eric Wan, and Simon Julier, "Sigma-point kalman filters for nonlinear estimation and sensor-fusion: Applications to integrated navigation," in *AIAA Guidance, Navigation, and Control Conference and Exhibit. August*, 2004.

[41] H. Krim and M. Viberg, "Two decades of array signal processing research," *IEEE Sig. Proc. Mag.*, 1996.

[42] P. Stoica and A. Nehorai, "MUSIC, Maximum Likelihood and Cramer-Rao Bound," *IEEE Trans. Acoust. and Sig. Proc.*, vol. 37, no. 5, 1989.

[43] J. X. Zhu and H. Wang, "Effects of sensor position and pattern perturbations on crlb for direction finding of multiple narrow-band sources," in *Spectrum Estimation and Modeling, 1988., Fourth Annual ASSP Workshop on*, Aug 1988, pp. 98–102.

[44] D. Tedaldi, A. Pretto, and E. Menegatti, "A robust and easy to implement method for imu calibration without external equipments," in *2014 IEEE International Conference on Robotics and Automation (ICRA)*, May 2014, pp. 3042–3049.

[45] S.O.H. Madgwick, A.J.L. Harrison, and R. Vaidyanathan, "Estimation of IMU and MARG orientation using a gradient descent algorithm," in *Rehabilitation Robotics (ICORR), 2011 IEEE International Conference on*, June 2011, pp. 1–7.

[46] Oliver J. Woodman, "An introduction to inertial navigation," Tech. Rep., 2007.

François Quitin is an Assistant Professor at the Université libre de Bruxelles (ULB), Belgium. He received the Ph.D. degree in Electrical Engineering from the Université Libre de Bruxelles (ULB), Brussels, Belgium and from the Université catholique de Louvain (UCL), Louvain-La-Neuve, Belgium in 2011. From 2011 to 2013, we was a post-doctoral researcher at the University of California, Santa Barbara (UCSB), and from 2013 to 2015, he was a postdoctoral research fellow at Nanyang Technological University, Singapore. He is the recipient of the 2012 Alcatel-Lucent Bell Scientific Award . His research interests focus on experimental and prototyping aspects in wireless communications, taking advanced theoretical ideas all the way to practice.

Philippe De Doncker received the M.Sc. degree in physics engineering and the Ph.D. degree in science engineering from the Universiteé libre de Bruxelles (ULB), Bruxelles, Belgium, in 1996 and 2001, respectively. He is currently a Professor with the ULB where he leads the research activities on wireless channel modeling and (bio-)electromagnetics.

François Horlin received the Ph.D. degree from the Université catholique de Louvain (UCL) in 2002. He specialized in the field of signal processing for digital communications. He joined the Inter-university Micro-Electronics Center (IMEC) in 2002. He led the project aiming at developing a 4G cellular communication system in collaboration with Samsung Korea. In 2007, François Horlin became professor at the Université libre de Bruxelles (ULB). He is currently supervising a research team working on next generation communication systems. Localization based on 5G signals, filterbank-based modulations, massive MIMO and dynamic spectrum access are examples of currently investigated research topics. He has been academic representative to the executive board of ULB from 2010 to 2015. Since 2017, he is vice dean for research at the Ecole Polytechnique de Bruxelles (EPB).

Wee Peng Tay (S'06 M'08 SM'14) received the B.S. degree in Electrical Engineering and Mathematics, and the M.S. degree in Electrical Engineering from Stanford University, Stanford, CA, USA, in 2002. He received the Ph.D. degree in Electrical Engineering and Computer Science from the Massachusetts Institute of Technology, Cambridge, MA, USA, in 2008. He is currently an Associate Professor in the School of Electrical and Electronic Engineering at Nanyang Technological University, Singapore. His research interests include distributed inference and signal processing, sensor networks, social networks, information theory, and applied probability.

Dr. Tay received the Singapore Technologies Scholarship in 1998, the Stanford University President's Award in 1999, the Frederick Emmons Terman Engineering Scholastic Award in 2002, and the Tan Chin Tuan Exchange Fellowship in 2015. He is a coauthor of the best student paper award at the Asilomar conference on Signals, Systems, and Computers in 2012, and the IEEE Signal Processing Society Young Author Best Paper Award in 2016. He is currently an Associate Editor for the IEEE Transactions on Signal Processing, an Editor for the IEEE Transactions on Wireless Communications, serves on the MLSP TC of the IEEE Signal Processing Society, and is the chair of DSNIG in IEEE MMTC. He has also served as a technical program committee member for various international conferences.